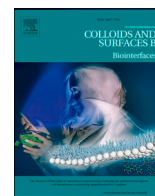




Contents lists available at ScienceDirect

Colloids and Surfaces B: Biointerfaces

journal homepage: www.elsevier.com/locate/colsurfb

PCL-fibrin-alginate hydrogel based cell co-culture system for improving angiogenesis and immune modulation in limb ischemia

Gyubok Lee^{a,1}, Yeong Hwan Kim^{b,1}, Dongwoo Kim^a, Dong-Hyun Lee^b, Suk Ho Bhang^{b,*}, Kangwon Lee^{a,*}

^a Department of Applied Bioengineering, Graduate School of Convergence Science and Technology, Seoul National University, Seoul 08826, Republic of Korea

^b School of Chemical Engineering, Sungkyunkwan University, Suwon 16419, Republic of Korea

ARTICLE INFO

Keywords:

Angiogenesis
Cell therapy
Immune modulation
Ischemic condition
Multilayer hydrogel

ABSTRACT

Stem cell therapy has demonstrated promise in regenerative medicine due to their ability to differentiate into various cell types and secrete growth factors. However, challenges such as poor survival rate of transplanted cells under ischemic and immune conditions limit its effectiveness. To address these issues, we developed a polycaprolactone (PCL)-fibrin-alginate matrix hydrogel, which combines adipose-derived stem cells and human umbilical vein endothelial cells with a PCL fiber, encapsulated within fibrin and alginate hydrogel to enhance cell survival, proliferation, and immune modulation. This structure offers protection to the encapsulated cells, supports angiogenesis, and modulates the immune response, significantly improving therapeutic outcomes in a mouse model of hindlimb ischemia. Our *in vitro* and *in vivo* results demonstrate the scaffold's ability to support cell viability, promote angiogenesis, and modulate inflammatory responses, indicating its potential as a promising platform for ischemic tissue repair and regenerative medicine. This innovative approach to cell-based therapy highlights the importance of scaffold design in enhancing the therapeutic efficacy of stem cell treatments for ischemic diseases.

1. Introduction

Stem cell therapy has emerged as a transformative approach in regenerative medicine, offering potential solutions for conditions with limited treatment options [1]. This field has gained significant momentum due to its ability to address complex medical issues that traditional treatments cannot effectively manage [2]. Among various stem cell types, adipose-derived stem cells (ADSCs) are known as a valuable resource for tissue repair and regeneration due to their ability to differentiate into multiple cell types and secrete a wide array of growth factors [3–5]. Specifically, ADSCs secrete factors such as vascular endothelial growth factor (VEGF), fibroblast growth factor (FGF), and hepatocyte growth factor (HGF), which are crucial for angiogenesis and tissue healing [6–8]. However, despite of the advantages, the clinical application of ADSCs faces challenges [9].

The hostile microenvironment of ischemic tissues, characterized by immune rejection and poor vascularization, presents significant challenges for cell survival and therapeutic efficacy [10]. High rates of

apoptosis in transplanted cells further diminish their regenerative potential. To overcome these limitations, recent research has prioritized strategies that directly promote vascular network formation and mitigate inflammatory responses for enhancing tissue regeneration and long-term therapeutic success. A recent study demonstrated that implanting a hydrogel with microchannel networks significantly improved blood perfusion to ischemic sites by forming functional vascular structures [11]. This approach showed therapeutic benefits in mouse and porcine models of hindlimb ischemia, where the microchannel networks facilitated pro-angiogenic M2 polarization of macrophages, leading to enhanced endothelial cell recovery and reduced inflammation. Similarly, recent study has explored the use of photocrosslinkable gelatin methacrylate (GelMA) hydrogels, which supported vascular network formation by incorporating human blood-derived endothelial colony-forming cells (ECFCs) and bone marrow-derived mesenchymal stem cells (MSCs) [12]. These cell-laden GelMA hydrogels formed extensive capillary-like networks *in vitro* and rapidly developed functional anastomoses with host vasculature *in*

* Corresponding authors.

E-mail addresses: sukhobhang@skku.edu (S.H. Bhang), kangwonlee@snu.ac.kr (K. Lee).

¹ These authors contributed equally to this work.

<https://doi.org/10.1016/j.colsurfb.2025.114553>

Received 3 November 2024; Received in revised form 10 December 2024; Accepted 2 February 2025

Available online 3 February 2025

0927-7765/© 2025 Elsevier B.V. All rights are reserved, including those for text and data mining, AI training, and similar technologies.

immunodeficient mice. Furthermore, the degree of GelMA methacrylation was shown to modulate vascularization and inflammatory responses, optimizing therapeutic outcomes. Another study focusing on acute myocardial infarction reported the development of an injectable hydrogel synthesized from chitosan modified by boronate-protected diazeniumdiolate, capable of releasing nitric oxide in response to reactive oxygen species [13]. This dual-function hydrogel demonstrated anti-inflammatory effects, reduced cardiac remodeling, and enhanced tissue repair, ultimately restoring cardiac function in a mouse model of myocardial ischemia/reperfusion injury. Another investigation reviewed the use of injectable anti-inflammatory hydrogels for treating acute myocardial infarction [14]. The study highlighted the potential of hydrogels to deliver various therapeutic molecules, including anti-inflammatory drugs, antioxidants, and immune-regulation drugs, to reduce inflammatory responses in ischemic conditions. Collectively, these studies highlight the potential of hydrogel-based scaffolds to address ischemic tissue repair through mechanisms that directly enhance vascularization and modulate inflammatory responses. By aligning our focus on these pivotal aspects, we aim to advance the therapeutic efficacy of regenerative materials for ischemic conditions.

Furthermore, there are concerns regarding the safety of stem cell therapies, including the risk of teratoma formation and the potential for unpredictable cell behavior [15], [16]. Recent research has focused on the development of hydrogel-based scaffolds to address these challenges [17]. Hydrogels, with their three-dimensional network of hydrophilic polymers, provide a supportive microenvironment that facilitates cell encapsulation, protection from immune rejection and extended cell survival [18]. For example, a study demonstrated that encapsulating ADSCs in a hydrogel matrix significantly improved their survival and function in a mouse model of myocardial infarction [19]. Hydrogels composed of materials such as fibrin, alginate, and polycaprolactone (PCL) have shown promise in enhancing cell survival, promoting angiogenesis, and modulating immune responses [20]. Among these, PCL provides robust mechanical properties and excellent structural integrity, making it an ideal candidate for load-bearing applications. However, its synthetic nature results in a lack of sufficient cell adhesion motifs, limiting its compatibility with cellular attachment and proliferation [21]. Studies have shown that PCL alone struggles to support effective cell integration, with evidence pointing to suboptimal tissue adhesion and regeneration outcomes [22,23]. This limitation highlights that PCL, when used alone, has certain constraints that make it challenging to meet the dual requirements of mechanical robustness and biological performance. On the other hand, fibrin, a natural biopolymer, is highly biocompatible and promotes cell adhesion and angiogenesis [24]. Specifically, when fibrin is in direct contact with cells, it promotes tube formation through integrin-mediated adhesion and interaction with cell surface receptors, such as integrins $\alpha v\beta 3$ and $\alpha 5\beta 1$ [25,26]. Despite these advantages, its intrinsic weakness in mechanical properties presents a significant challenge. Fibrin scaffolds often fail to maintain structural stability under physiological conditions, making them unsuitable for standalone use [27]. While alginate provides a biocompatible matrix that shields cells from immune attack [28], it inherently lacks cell adhesion motifs, which limits its ability to support effective cell attachment and proliferation. This limitation makes alginate biologically suboptimal for tissue regeneration without additional modifications to enhance its compatibility for cellular interactions [29,30]. Therefore, it is essential to develop complementary combinations of scaffolds that can offset the individual weaknesses of each material while maximizing their respective strengths to achieve optimal performance in regenerative applications. Furthermore, studies using similar materials, such as alginate and fibrin, have consistently demonstrated long-term cell viability, with survival rates remaining high beyond two to three weeks, underscoring the potential of these materials to support sustained cellular function in therapeutic applications. [31–33].

The co-culture of ADSCs with human umbilical vein endothelial cells (HUVECs) within these hydrogel scaffolds has been shown to enhance

cell proliferation and angiogenic potential [34]. For instance, *in vitro* studies have demonstrated that co-culturing ADSCs with HUVECs leads to increased secretion of VEGF and improved formation of capillary-like structures [35]. Co-culturing allows for paracrine signaling between ADSCs and HUVECs, which is crucial for the secretion of angiogenic factors and the promotion of vascular networks [36]. However, creating a stable and supportive environment for both cell types under ischemic conditions remains a challenge [37]. Ischemic conditions, such as those found in critical limb ischemia (CLI), pose a significant barrier to effective stem cell therapy [38]. CLI is a severe form of peripheral arterial disease where blood flow to the limbs is critically reduced, leading to severe pain, ulcers, and even gangrene [39]. In CLI, reduced blood flow leads to tissue necrosis and a hostile microenvironment for transplanted cells [40]. The survival rate of stem cells in such environments is notably low due to oxidative stress, inflammation [41]. This underscores the need for a delivery system that not only supports cell viability but also enhances the therapeutic potential of stem cells [42].

In this study, we developed an innovative multilayer hydrogel cage to address the limitations of current stem cell therapies. This advanced structure incorporates HUVECs and ADSCs within PCL fibers embedded in a fibrin hydrogel, encapsulated by an outer layer of alginate hydrogel. The PCL fibers provide robust mechanical support, ensuring structural integrity for implantation in ischemic tissues, while the fibrin enhances cell adhesion and promotes angiogenesis, crucial for tissue regeneration. The outer alginate layer acts as a protective barrier, shielding encapsulated cells from the host immune system while maintaining scaffold stability. This multilayer hydrogel cage supports cell survival, and proliferation, and creates an optimal environment for tissue repair. By combining materials that offer mechanical strength and biocompatibility, our hydrogel cage aims to enhance the therapeutic potential of co-cultured ADSCs and HUVECs, paving the way for more effective treatments for ischemic conditions. Extensive *in vitro* tests are conducted to evaluate improvements in cell viability, proliferation, and angiogenic factor secretion, as well as the scaffold's ability to modulate immune responses and support tissue healing. This study presents a promising new direction in stem cell therapy for ischemic conditions, potentially offering significant advancements in regenerative medicine and paving the way for future clinical applications.

2. Materials and methods

2.1. Cell culture

Human adipose derived stem cells (ADSCs) were acquired from CEFO, Seoul, republic of Korea. These cells were isolated from healthy human adipose tissue collected via liposuction or surgical excision, with the procurement process receiving approval from CEFO's Ethical Committee (approval number CB-IRB-120224). Human umbilical vein endothelial cells (HUVECs) were procured from Lonza Incorporation (Bazel, Switzerland). The cells were propagated in T-75 flasks and kept at 37 °C in a humidified chamber with 5 % CO₂ atmosphere. ADSCs were grown in Dulbecco's Modified Eagle Medium (DMEM), enriched with 10 % fetal bovine serum (FBS, Cellsera, Australia) and 1 % antibiotic-antimycotic solution (Welgene, Gyeongsan, Korea). HUVECs were maintained in Endothelial Basal Medium (EBM-2) provided by Lonza, fortified with an Endothelial Growth Supplement (EGM-2, Lonza) and 1 % antibiotic-antimycotic solution.

2.2. Preparation of PFA scaffold with embedded cells

The creation of hydrogels began with the production of PCL fibers using an electrospinning technique. A 20 % (w/v) PCL solution (Molecular Weight: 80,000; Sigma Aldrich, St. Louis, MO, USA) was dissolved in 2,2,2-trifluoroethanol (TFE). This solution was dispensed through an 18 G stainless steel needle, connected to a syringe pump, and charged with a 7.5 kV potential, at a flow rate of 0.8 mL/h for 30 mins.

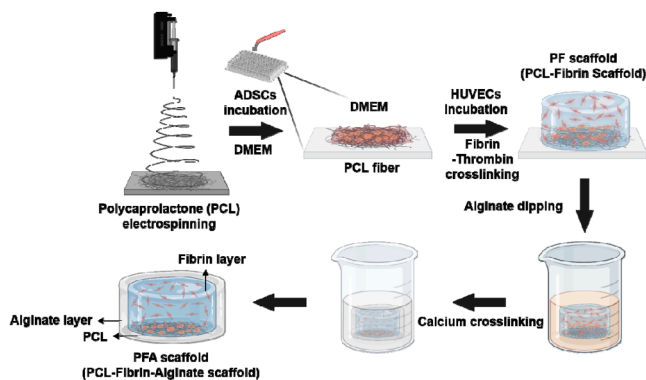


Fig. 1. Schematic illustration of PCL-fibrin-alginate (PFA) scaffold fabrication.

The PCL fibers were crafted into 5 mm squares with precision cutting tools and placed into a 96-well culture plate. To load ADSCs onto the scaffold, 1.25×10^5 ADSCs were suspended in 20 μL of DMEM and carefully pipetted directly onto each PCL nanofiber square. These were incubated for 30 mins at 37 °C in a 5 % CO_2 atmosphere to allow efficient cell attachment to the fibers. Following ADSC incubation, a fibrin-thrombin hydrogel containing HUVECs was prepared to form the endothelial layer. Specifically, 2.5×10^5 HUVECs were suspended in an 80 μL fibrinogen solution (20 mg/mL in phosphate-buffered saline, PBS). The fibrinogen solution was gelled by adding 8 μL of thrombin (2.5 U/mL in 20 mM CaCl_2) and allowed to crosslink for 30 mins at 37 °C. The fibrin-thrombin hydrogel was then layered over the ADSC-incubated PCL sheet, ensuring even coverage and integration. Finally, the composite PCL-fibrin scaffold was carefully removed using a specialized tool and coated with an alginate hydrogel to form the outer layer. This was achieved by immersing the scaffold in a 6-well plate filled with 5 mL of a 1 % (w/v) sodium alginate solution, followed by the addition of 5 mL of a 1 % (w/v) calcium chloride solution to initiate gelation. Crosslinking was completed within 30 s at ambient conditions (Fig. 1).

2.3. Characterization of the PFA scaffold for limb ischemia therapy

For the evaluation of scaffolds tailored for heart tissue repair, a high-definition CCD camera was employed for initial visualization and spatial analysis. The scaffolds were placed 10 cm from the device's lens for optimal image capture. Detailed examinations of the external scaffold architecture were conducted with a Helios 5 UC SEM system (Thermo Fisher Scientific, Hillsboro, OR, USA), following sputter deposition of a fine platinum coating on the scaffold surfaces for enhanced electron imaging. SEM analyses were performed at an operating voltage of 10 kV to capture fine details of the scaffold's surface morphology. The mechanical properties of the various scaffold configurations were assessed for their compressive behavior using an Instron 3343 mechanical testing unit (Instron Corporation, Norwood, MA, USA). The scaffolds, including the fibrin hydrogel, PCL-fibrin hydrogel, and PFA hydrogel, were equilibrated in PBS for 30 mins to reach full saturation. Excess moisture was carefully eliminated from each scaffold before testing. Data on stress and deformation were gathered under compressive loads, allowing for accurate stress-strain curve generation. To characterize the viscoelastic nature of these materials, dynamic mechanical analysis was implemented. Samples were arranged between metal plates of 2 cm diameter, ensuring a 1 cm separation for consistent application of shear forces. Their dynamic response to shear forces was analyzed with an MCR 102 rheometer (Anton Paar, Graz, Austria), focusing on the storage modulus. A steady shear strain of 10 % was applied across a frequency sweep from 0.1 to 300 Hz (rad/s) at a stable temperature of 25 °C, providing insights into the samples' elastic storage capacity under cyclic loading conditions.

2.4. Swelling and degradation test

The swelling test for hydrogel samples was conducted to evaluate their ability to absorb and retain fluids. Initially, the hydrogels were dried in an oven set to 70 °C overnight. Following this drying process, they were rehydrated using a phosphate-buffered saline solution (PBS, Welgene). Any surplus PBS on the hydrogel surface was gently removed with filter paper. The weight of each hydrogel sample was measured three times at regular intervals, with all measurements conducted at a consistent temperature of 37 °C. The key metric calculated from this test is the swelling ratio (SR) of the hydrogels. This ratio is determined using the formula $\text{SR} = (W_t - W_0) / W_0 \times 100$, where W_t is the weight of the hydrogel after it has swollen at a certain time point, and W_0 is its initial dry weight before rehydration. This formula and the resulting swelling ratio provide a quantitative insight into the hydrogel's capacity to absorb and retain liquid, which is critical for its intended applications.

The degradation test was conducted to evaluate the stability and degradation behavior of hydrogel scaffolds over a 2-week period under simulated physiological conditions. The preparation of scaffolds for this test followed the same procedure as described for the preparation of PFA scaffolds. After preparation, the scaffolds were incubated in phosphate-buffered saline (PBS, Welgene) at 37 °C. To assess weight changes due to degradation, the scaffolds were carefully removed from the PBS each day, and excess surface water was gently removed by rolling them on tissue paper. This step ensured that only the scaffold's remaining weight, free from external surface moisture, was recorded. The weight of each scaffold was measured daily throughout the 2-week period.

2.5. Biocompatibility test

The biocompatibility evaluation of hydrogel composites on various cell types, including ADSCs and HUVECs, was conducted using an indirect method based on hydrogel extracts, in alignment with the ISO 10993-12 guidelines. Briefly, the hydrogel extracts were produced by immersing the hydrogel composite in a serum-free medium, with a concentration of 0.2 g/mL, and incubating it for 48 hrs at 37 °C. For the LIVE/DEAD assay, ADSCs and HUVECs were cultivated in 24-well plates at a density of 50,000 cells per well for 48 hrs. The cells were then exposed to the hydrogel extract solution prepared as mentioned earlier. The viability of these cells was monitored on days 1, 4, and 7. This was achieved by administering 2 μM of Calcein AM and 4 μM of Ethidium Homodimer-1 30 mins before conducting fluorescence imaging at room temperature. These observations were further validated using a laser scanning microscope from Carl Zeiss (Oberkochen, Germany). To directly assess biocompatibility, ADSCs and HUVECs were separately integrated and cultured inside the scaffolds for 7 days. The cells were then treated with Calcein AM and 4 μM Ethidium Homodimer-1 for 30 mins. Fluorescence imaging was then conducted to gather further insights.

2.6. In vitro analysis of cell growth on the scaffold

The *in vitro* cell proliferation evaluation on scaffolds was conducted using the WST assay method (EZ-Cytox, DoGenBio, Korea). Scaffold extracts were generated by immersing the scaffold composite in a medium enriched with 10 % FBS at a density of 0.2 g/mL and incubating it for 48 hrs at 37 °C. The scaffolds were first sterilized using 0.1 % acetic acid (Sigma-Aldrich) and then thoroughly rinsed in sterile PBS for 3 hrs. ADSCs and HUVECs were cultured at a density of 50,000 cells per well in 24-well plates for 48 hrs. The cells were treated with the scaffold extract solution, and cell proliferation was observed on days 1, 4, and 7 with the absorbance at 450 nm using a microplate reader (Synergy H1, BioTek, Vermont).

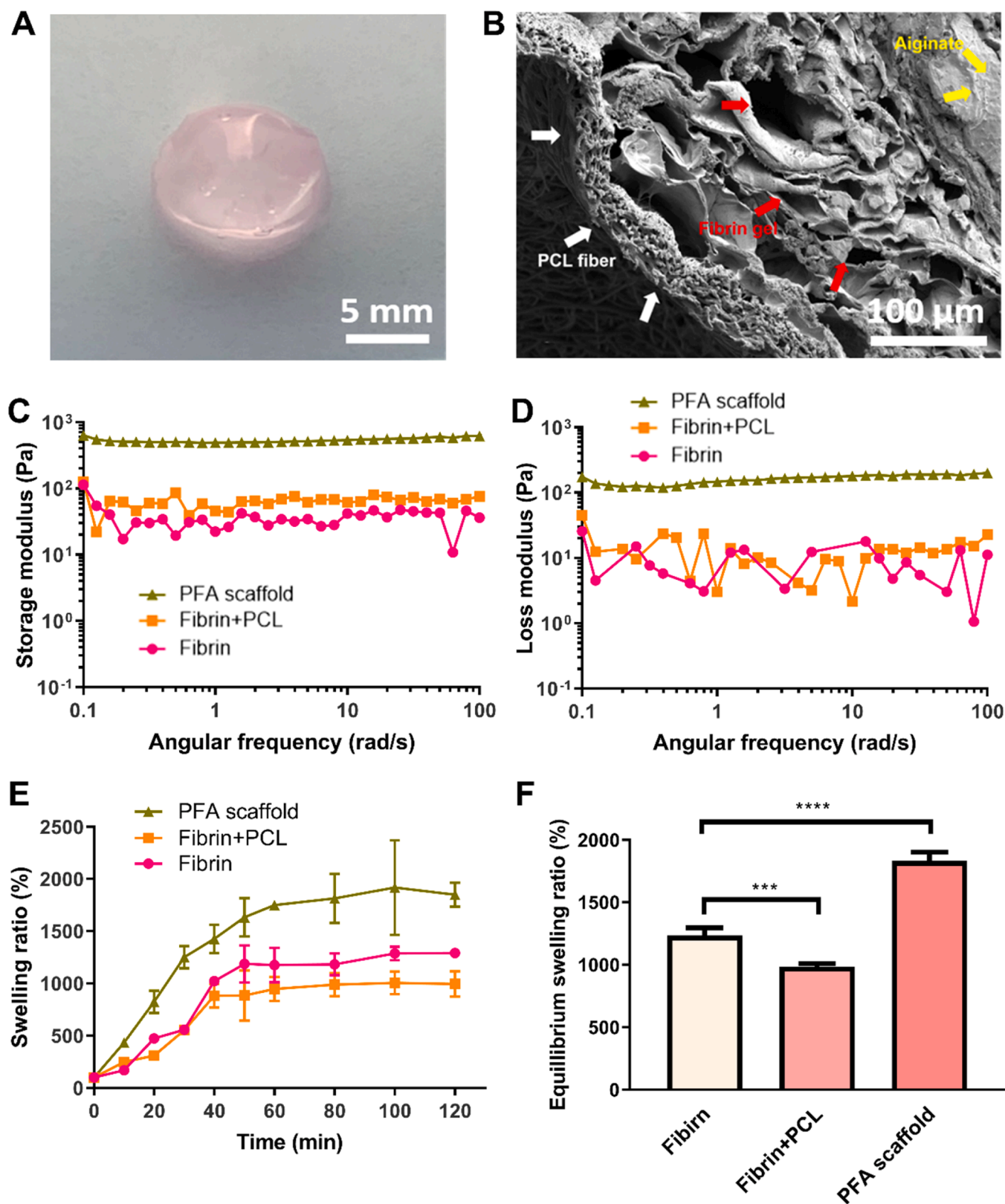


Fig. 2. Characterization of the PFA scaffold composed with electrospun fibers and two separate hydrogel layers aimed to enhance the angiogenesis. (a) Digital camera images of the PFA scaffold (scale bar = 5.0 mm). (b) Representative SEM image illustrating the compartmentalized architecture of the PFA scaffold (scale bar = 100 μm). (c) The storage modulus of the scaffolds depending on the components. (d) The loss modulus of the scaffolds depending on the components. (e) Swelling ratio (n = 3) and (f) equilibrium swelling ratio (n = 5) of the scaffolds at different swelling intervals, ***p < 0.001, ****p < 0.0001 versus fibrin group.

2.7. Real-time quantitative polymerase chain reaction (qRT-PCR) analysis

Total RNA was extracted from the cells *in vitro* experiment and the tissue in ischemic limb *in vivo* experiment using the TRIzol method. Total RNA was reverse transcribed into complementary DNA (cDNA), and qRT-PCR was conducted using the SYBR Green system (Thermo Fisher, Waltham, MA, USA) and the QuantStudio 5 system (Applied Biosystems, Waltham, MA, USA), following the manufacturer's protocol. The relative expression levels of human *GAPDH*, *MMP1*, *VEGFR*, *CD31*, *FGF2*, and mouse β -actin, *CD31*, α -SMA, *TGF β -1*, *IL-1 β* , *IL-6* were assessed. Human-specific gene primers were used for the *in vitro* cell analysis. Mouse gene primers were used for *in vivo* mouse ischemic limb analysis. Detailed primer sequences for the various genes can be found in [Table S1](#) and [S2](#).

2.8. Tube formation assay

To evaluate the angiogenic potential of the scaffolds for tissue regeneration, an *in vitro* tube formation assay was conducted. Growth factor-reduced matrigel (Corning Incorporated, New York, NY, USA) was evenly spread across each well to create a basement membrane matrix layer. The coated well plate was incubated at room temperature for 30 mins, followed by further incubation in a humidified atmosphere (5 % CO₂, 37 °C) for 1 hr. HUVECs were seeded into each well and cultured for 16 hrs using a transwell system alongside a multilayer scaffold incorporating scaffold alone, HUVECs alone, and HUVECs with ADSCs. After a 16 hrs incubation period, the formed tubular structures were imaged using a microscope. ImageJ software was employed to count the tubular nodes and junctions.

2.9. Analysis of proinflammatory cytokines in mouse macrophages using enzyme-linked immunosorbent assay (ELISA)

RAW 264.7 macrophage cell line (ATCC, Manassas, VA, USA) was cultured at a density of 5×10^4 cells per well in 24-well plates and incubated for 24 hrs in preparation for the analysis of proinflammatory cytokines using ELISA. After the incubation period, the cells were exposed to various scaffold eluates and 1 μ g/mL lipopolysaccharide (LPS). Following 24 hrs of treatment, the culture supernatant was collected and subjected to centrifugation to eliminate any cellular debris. The concentrations of proinflammatory cytokines, including TNF- α (Abcam, Cambridge, UK), IL-1 β (Abcam), and IL-6 (Abcam), were quantitatively measured using dedicated ELISA kits.

2.10. Immunoblotting analysis of protein expression

For *in vitro* inflammatory factor expressions analysis, the RAW 264.7 macrophage cell line (ATCC) was purchased and cultured with various scaffold eluates for 6 and 24 hrs durations. After the scaffold eluates treatment, the cells were rinsed and lysed using RIPA buffer (Sigma Aldrich) supplemented with Xpert phosphatase inhibitor cocktail solution (GenDEPOT, Barker, TX, USA). For *in vivo* immune modulatory effect analysis, the tissue in ischemic limb *in vivo* experiment was completely lysed with RIPA buffer supplemented with Xpert phosphatase inhibitor cocktail solution for protein extraction. The proteins were separated by 10 % SDS-PAGE and transferred onto PVDF membranes. The membranes were blocked with 5 % skim milk and then incubated with primary antibodies. The primary antibodies included β -actin (Cell Signaling, Beverly, MA, USA), TGF- β (Cell Signaling), IL-1 β (Abcam), GAPDH (Abcam), CD206 (Abcam), TNF- α (Cell Signaling), and IL-6 (Cell Signaling). Following incubation with primary antibodies, the membranes were exposed to a secondary antibody (Abcam). Protein bands were visualized on PVDF membranes using a Las 4000 device (Fujifilm, Tokyo, Japan) and Clarity Western ECL substrate (Bio-Rad, Hercules, CA, USA).

2.11. Mouse hindlimb ischemia model

Four-week-old female athymic mice (ICR strain, 20–25 g, obtained from Orient, Seongnam, Gyeonggi, Korea) were anesthetized using xylazine (10 mg/kg, Bayer, Seoul, Korea) and ketamine (100 mg/kg, Yuhan, Seoul, Korea). The femoral artery along with its branches was tied off using 6–0 silk sutures (AILEE, Busan, Korea). Additionally, the external iliac artery and all proximal arteries were ligated. The femoral artery was removed from its origin at the external iliac artery to its division into the saphenous and popliteal arteries. All animal protocols and experimental procedures were approved by the Institutional Animal Care and Use Committee of Sungkyunkwan University (Approval No. SKKUIACUC2020–12–41–1).

2.12. Histological analysis *in vivo*

Tissues from the ischemic limb were collected 28 days after the various treatments and embedded in optimal cutting temperature compound (SciGen Scientific Inc., Gardenas, CA, USA), frozen at -22 °C, sliced into 10 μ m-thick sections. The sections underwent staining with hematoxylin and eosin (H&E) as well as Masson's Trichrome (MT) to assess muscle damage and inflammation.

2.13. Immunohistochemistry *in vivo*

The tissue sections were stained using anti-CD31 and anti-SM α -actin antibodies (Abcam). Signals were visualized with fluorescein isothiocyanate-conjugated secondary antibodies (Jackson Immuno Research Laboratories, West Grove, Pennsylvania, USA). The sections were counterstained with DAPI and observed using a fluorescence microscope (DMi8, Leica).

2.14. Statistical analysis

The data are reported as mean values with accompanying standard deviations. Statistical analysis was performed using GraphPad Prism 8 software (GraphPad, San Diego, CA). Group comparisons were conducted using one-way ANOVA, followed by post hoc multiple comparison tests with a 95 % confidence interval. Statistical significance was indicated by P-values less than 0.05.

3. Results and discussion

3.1. Characterization of the composite scaffold for limb ischemia therapy

In this study, we have developed a novel composite scaffold incorporating alginate, fibrin, and PCL, demonstrating significant potential in the treatment of limb ischemia. Our scaffold, characterized by its unique hemispherical form and microscale structure, exhibits properties conducive to tissue integration and cellular interaction. Our investigation into a composite scaffold for treating limb ischemia has provided a detailed characterization of its structural and mechanical attributes, crucial for its intended biomedical application. The scaffold combines alginate, fibrin, and PCL, each contributing distinct properties that synergize within the scaffold group. The CCD camera image ([Fig. 2A](#)) shows the scaffold's macrostructure, presenting a hemispherical form indicative of our precision engineering to create a consistent and clinically relevant size of 5 mm. This size is carefully considered to maximize coverage and integration with the host tissue while minimizing invasiveness. In addition, the fibrin-only scaffold exhibits significantly weaker structural integrity compared to the composite PFA scaffold ([Figure S1](#)). This underscores the necessity of integrating alginate and PCL into the composite, which collectively enhance the scaffold's mechanical robustness and suitability for biomedical application. The SEM image ([Fig. 2B](#)) provides a microscale perspective, revealing the scaffold's highly organized internal structure. The PCL fiber provides a basic

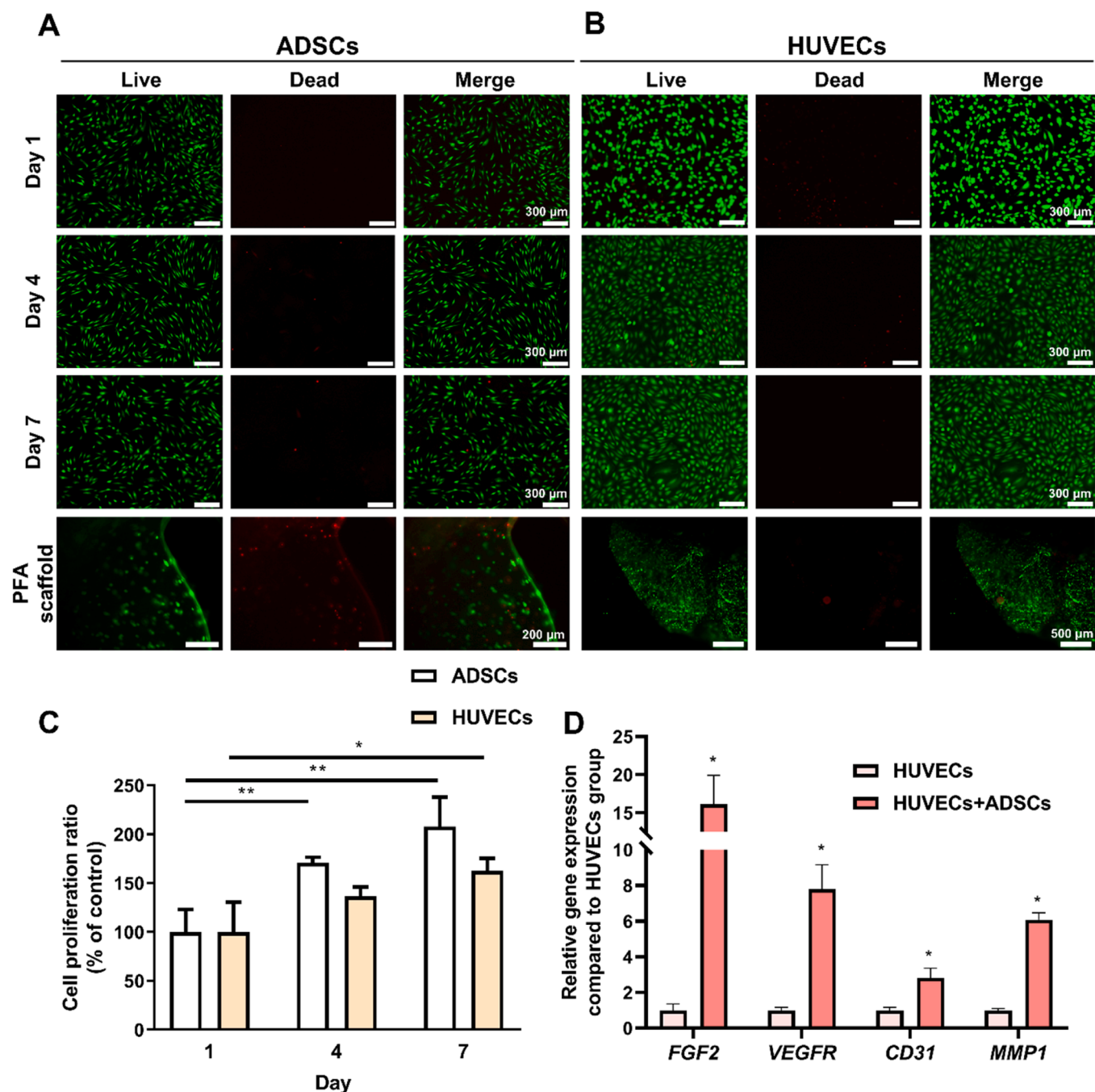


Fig. 3. Evaluating biocompatibility and enhanced angiogenic capacity based on PFA scaffold. Representative fluorescence images of the live (green) and dead (red) (a) ADSCs and (b) HUVECs cultured with PFA scaffold or eluate from the scaffold as evaluated by FDA/EB staining. Scale bars = 200 μ m. (c) Cell proliferation ratio of ADSCs and HUVECs when cultured with PFA scaffold eluates ($n = 3$, * $p < 0.05$, ** $p < 0.01$ versus each cell type on day 1, control: WST assay results for each cell on day 1). (d) qRT-PCR results showing representative angiogenic markers (VEGFR, CD31, FGF2) and the migratory marker (MMP1) from HUVECs and HUVECs cocultured with ADSCs (day 3, $n = 3$, * $p < 0.05$ versus HUVECs group).

cell adhesion matrix that supports the initial cell attachment of ADSCs [43]. The fibrin, identified by the red arrows, forms a fibrous network reminiscent of the body's natural extracellular matrix, essential for supporting cell attachment and migration. This network is reinforced by the alginate, which imparts the necessary mechanical strength and structural integrity, ensuring the scaffold's stability within the dynamic environment of the limb.

The rheological assessment of the composite scaffold reveals critical insights into its mechanical behavior and potential for clinical application in limb ischemia therapy. Specifically, the storage modulus profile (Fig. 2C) highlights the PFA scaffold's excellent elasticity, maintaining a

high modulus over a wide range of angular frequencies. This high storage modulus indicates that the scaffold possesses a robust structure, capable of withstanding significant deformation before yielding, superior to the values of fibrin and fibrin + PCL scaffolds. The PFA scaffold exhibits an enhanced modulus compared to fibrin alone, highlighting the alginate's role in augmenting the composite's structural rigidity. The loss modulus data (Fig. 2D) provides a measure of the scaffold's ability to dissipate energy through internal friction. The lower loss modulus, compared to the storage modulus, indicates a material that, while elastic, can absorb and dissipate energy from dynamic loads, such as those experienced during limb movement [44]. This property is crucial

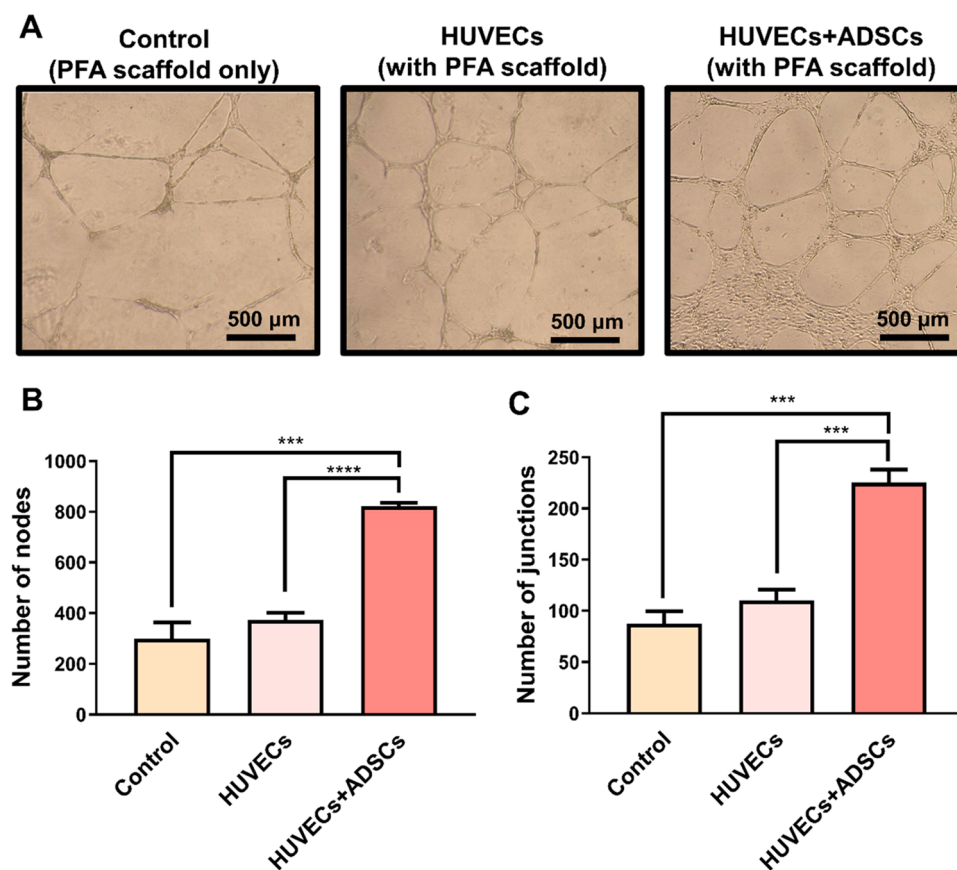


Fig. 4. Angiogenic potential of PFA scaffold as evaluated by *in vitro* tube formation assay using HUVECs in a transwell system. (a) Representative light microscope images showing tube formation from HUVECs cultured with PFA scaffold (scale bars = 500 μ m). (b) The number of nodes formed in the assay with different cell types (n = 3). (c) The number of junctions formed in the assay with different cell types (n = 3). * **p < 0.001, * ** *p < 0.0001 versus each group.

for scaffolds designed to interface with soft tissue, suggesting a material that can conform to the changing mechanical environment without causing damage to the surrounding or embedded cells. Additionally, the degradation profile demonstrates that while the PF scaffold is almost completely degraded within 3–4 days, the alginate-coated PFA scaffold retains over 70 % of its weight for more than a week, underscoring the critical role of alginate in enhancing structural stability (Figure S2).

For swelling behavior, the time-dependent swelling ratio (Fig. 2E) demonstrates that the PFA scaffold's rate of fluid absorption is rapid and reaches a plateau that exceeds the swelling capacity of fibrin and fibrin + PCL scaffolds. This indicates the interconnected porous structure facilitated by the presence of alginate, which allows for substantial fluid intake, essential for nutrient transport and metabolic waste removal in a cellular environment. Finally, the equilibrium swelling ratio (Fig. 2F) provides a long-term perspective on the scaffold's fluid management capability. The PFA scaffold significantly outperforms the individual components, achieving a swelling ratio that underscores the synergistic effect of combining alginate, fibrin, and PCL. This elevated swelling capacity at equilibrium suggests that the scaffold can maintain a more hydrated state over extended periods, which is beneficial for absorbing exudate. The PFA composite scaffold's rheological properties and swelling behavior are optimized to support the dynamic mechanical stresses of limb tissues while providing a conducive environment for cellular processes, making it an excellent candidate for limb ischemia therapy.

3.2. Cytocompatibility and functional analysis of PFA scaffold for enhanced angiogenesis in limb ischemia therapy

The PFA scaffold designed for limb ischemia therapy was subjected

to rigorous cytocompatibility assessments to determine its support for cell viability and angiogenic potential. Live/Dead assays conducted on ADSCs and HUVECs revealed a high proportion of viable cells (green fluorescence) over dead cells (red fluorescence) across all time points (1, 4, and 7 days), with notably higher viability observed within the scaffold similar with the eluate (Fig. 3A and B). This indicates a supportive cellular microenvironment offered by the scaffold's architecture. Cell proliferation assays quantitatively demonstrated that both ADSCs and HUVECs exhibited progressive growth over 7 days (Fig. 3C). The increased proliferation of HUVECs is particularly indicative of the scaffold's potential to support endothelialization, a critical step in angiogenesis. To further evaluate the cytocompatibility of the PFA scaffold in a co-culture system, ADSCs and HUVECs were co-cultured, and Live/Dead assays were conducted (Figure S3). The results demonstrated high cell viability and supportive interactions across all time points (1, 4, and 7 days). This indicates that the scaffold provides an optimal microenvironment for both cell types within the co-culture system. Furthermore, 3D live/dead imaging corroborated these findings, showing consistent cell viability in ADSCs and HUVECs co-cultured within the PFA scaffold over 1, 4, and 7 days, highlighting its robust and supportive environment for cellular activity (Figure S4). Quantitative analysis of cell viability revealed that the PFA scaffold consistently supported over 90 % live cell populations in ADSCs and HUVECs co-culture across all time points, underscoring its potential for angiogenic applications (Figure S5). The gene expression analysis further corroborated the beneficial impact of co-culture on angiogenesis within the scaffold. The co-culture approach significantly upregulated angiogenic and endothelial markers, emphasizing the importance of cell-cell interactions in enhancing angiogenesis, a key component in treating limb ischemia. There was a significant upregulation of angiogenic markers,

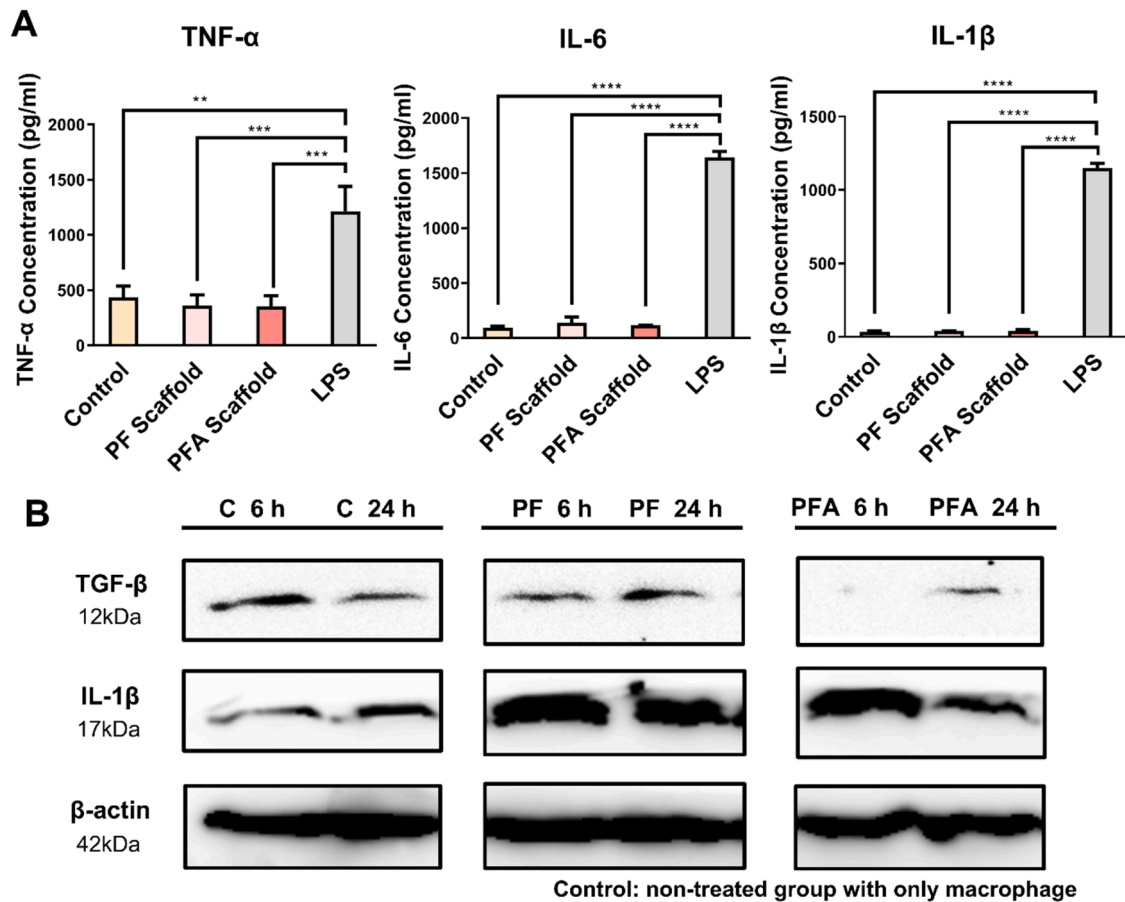


Fig. 5. Evaluating *in vitro* inflammatory factor expressions induced by the PFA scaffold. (a) ELISA results showing TNF- α , IL-6, and IL-1 β expression levels in macrophages treated with PF scaffold, PFA scaffold, and LPS ($n = 4$, ** $p < 0.01$, *** $p < 0.001$, **** $p < 0.0001$ versus LPS group, control: non-treated group with only macrophage). (b) Western blot results showing anti-inflammatory (TGF- β) and proinflammatory (IL-1 β) expression levels macrophages in control (C), PF scaffold (PF), and PFA scaffold (PFA) groups at 6 and 24 hrs after the eluates treatment.

FGF2 and VEGFR, in HUVECs when co-cultured with ADSCs, as opposed to HUVECs cultured independently. The endothelial marker CD31 and the matrix remodeling enzyme MMP1 also showed substantial upregulation in the co-culture group (Fig. 3D), delineating the collaborative effect on endothelial marker expression and potential for capillary formation [45]. The statistically significant upregulation of these genes in the co-culture condition (p -values < 0.05 for FGF2, and < 0.01 for VEGFR, CD31, and MMP1) provides strong evidence of the PFA scaffold's ability to foster a cellular environment that is not only favorable for individual cell types but also for the synergistic interaction between them, which is essential for effective angiogenesis. To further analyze the increase in angiogenesis markers due to co-culture, we further analyzed factors according to cell co-culture in 2D and 3D environments. Co-culturing of HUVECs with ADSCs in 3D scaffold significantly enhances the cellular expression of hypoxia-inducible factor-1 alpha (HIF-1 α) and VEGF, key markers implicated in angiogenesis (Figure S6). As illustrated in the accompanying bar graphs, the relative mRNA expression levels of HIF-1 α increased markedly in 3D HUVECs+ADSCs co-cultures compared to 2D conditions. Similarly, VEGF expression levels were notably elevated in the 3D co-culture system. These findings suggest that the 3D scaffold provides a conducive microenvironment that promotes cellular behaviors associated with hypoxia response and angiogenic signaling, potentially offering a substantial benefit over conventional 2D culture systems in tissue engineering applications [46]. In summary, the data compellingly demonstrate that the PFA scaffold, through the co-culture of ADSCs and HUVECs, distinctly promotes an angiogenic milieu. This scaffold is thereby validated as a potent enabler of the intricate cellular choreography required for angiogenesis,

essential for the restoration of blood flow in limb ischemia therapy.

3.3. Enhanced angiogenic potential of co-cultured PFA scaffold evidenced by *in vitro* tube formation

in vitro tube formation assays illustrated an enhanced angiogenic response, evident in the increased complexity and quantity of capillary-like structures, especially in the HUVECs+ADSCs co-culture group. The angiogenic potential of the PFA scaffold was further investigated through *in vitro* tube formation assays, providing a representative assessment of the scaffold's ability to support capillary-like structure formation. The presence or absence of the scaffold itself, without cells, showed no significant differences in tube formation (Figure S7). Microscopic analysis of the tubulogenesis within the control group, HUVECs group, and the HUVECs + ADSCs co-culture group illustrated a stark contrast in the complexity of the tube-like networks formed (Fig. 4A). The control group exhibited a baseline level of tube formation, while the HUVECs group demonstrated a significant increase in the number of nodes and junctions, indicative of endothelial cell activity. However, the most substantial enhancement was observed in the HUVECs + ADSCs group, which showed a marked increase in the complexity and quantity of the network structures, with the number of nodes and junctions dramatically exceeding those in the HUVECs-only group (Figs. 4B and 4C). Quantitative analysis revealed that the HUVECs + ADSCs group had significantly higher nodes and junctions compared to both the control and HUVECs only groups. The high expression of angiogenesis proteins such as CD31 within the PFA scaffold can be confirmed through fluorescence-stained tube images

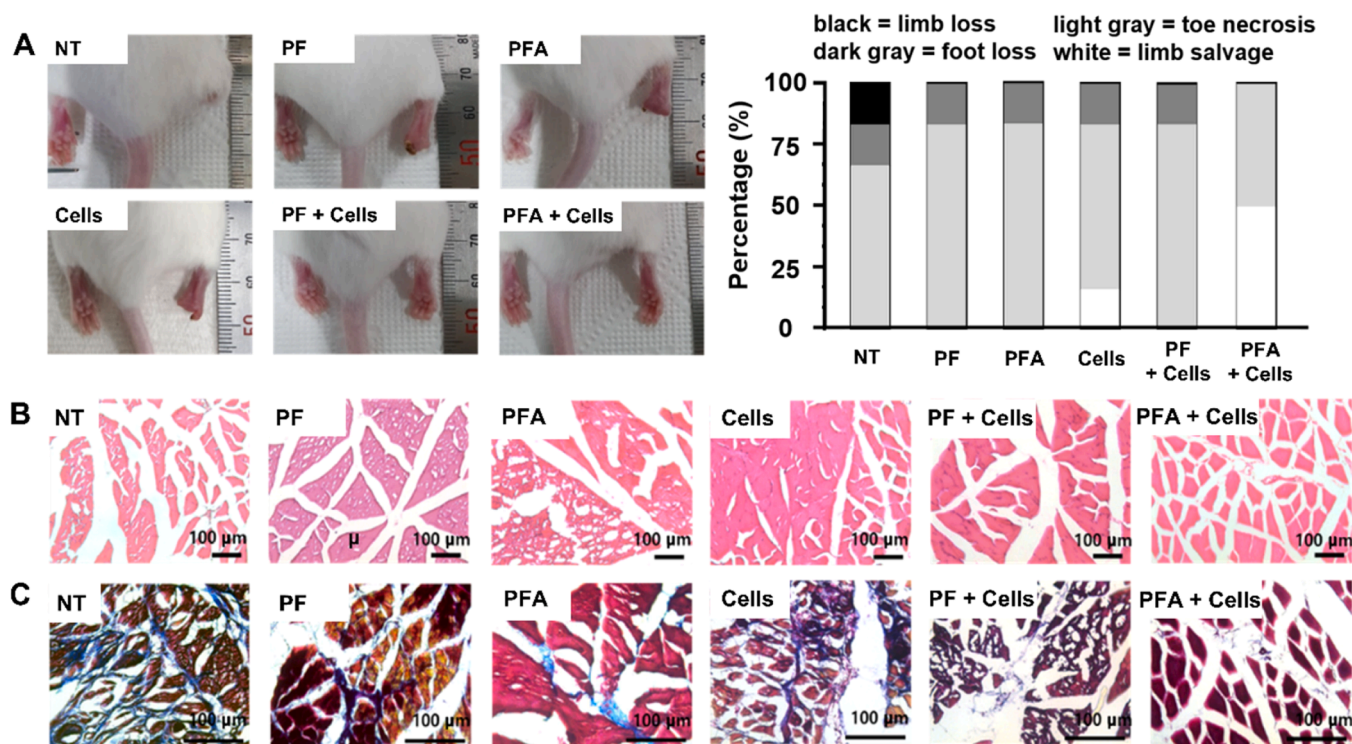


Fig. 6. Decreased inflammation, muscle degeneration, and limb loss by treating PFA scaffold (28 days after surgery). (A) Representative limb images with limb salvage ratio after the various treatments (black = limb loss, dark gray = foot loss, light gray = toe necrosis, white = limb salvage, percentage of total number of animals in each group, $n = 6$). Representative histological images of (B) H&E and (C) MT staining of ischemic lesions. (NT: no treatment, PF: PF scaffold only, PFA: PFA scaffold only, Cells: HUVECs + ADSCs, PF + Cells: PF scaffold with HUVECs + ADSCs, PFA + Cells: PFA scaffold with HUVECs + ADSCs, scale bars = 100 μm).

(Figure S8). The data suggests that the presence of ADSCs in the culture is synergistic, enhancing the angiogenic behavior of HUVECs, which is critical for the formation of a stable and functional capillary network [47]. This marked increase in tubulogenesis within the HUVECs + ADSCs group, compared to the HUVECs alone, underscores the importance of cellular interplay within the scaffold environment for promoting angiogenesis. In conclusion, the PFA scaffold not only supports individual endothelial cell function but also significantly amplifies the collective angiogenic potential when HUVECs are co-cultured with ADSCs. This synergistic interaction within the scaffold underscores its promising application in therapeutic angiogenesis, necessary for effective treatment of limb ischemia [48].

3.4. *In vitro* inflammatory cytokine analysis in PFA scaffold

Our scaffold exhibited an ability to modulate inflammatory responses. The inflammatory response elicited by the PFA scaffold was scrutinized using *in vitro* assays to measure the concentration of representative cytokines associated with inflammation. ELISA results demonstrated that the levels of pro-inflammatory cytokines (TNF- α , IL-6, and IL-1 β) were significantly lower in the PFA scaffold and PF groups compared to the LPS group, which served as a positive control for inflammation (Fig. 5A). Western blot analyses of TGF- β and IL-1 β supported these findings, with the PFA scaffold group showing a decrease in the pro-inflammatory cytokine (IL-1 β) and increase in the anti-inflammatory cytokine (TGF- β) relative to the control and fibrin groups at the investigated time points (Fig. 5B). Notably, the PFA scaffold group exhibited a pronounced reduction in pro-inflammatory cytokines at both 6 and 24 hrs post-elution, suggesting that the scaffold's composition might modulate the inflammatory response favorably. The control group showed basal levels of these cytokines, establishing a benchmark for comparison. The PF scaffold group displayed a moderate increase in IL-1 β levels, indicating basal inflammatory property.

However, the cytokine levels in PFA scaffold group were lower than both control and PF scaffold groups at 24 hrs, indicating the superior performance in mitigating an inflammatory response in PFA scaffold. This can be expected to alleviate the inflammatory response by preventing the outflow of contents within the PFA scaffold [49]. The significant reduction in pro-inflammatory cytokines in the PFA scaffold group underlines the potential of the scaffold to modulate inflammatory responses, which is critical for the prevention of chronic inflammation that can impair healing and tissue regeneration [50]. In summary, the PFA scaffold demonstrates an inherent capability to attenuate inflammatory responses, highlighting its suitability for therapeutic applications in tissue engineering where inflammation control is paramount.

3.5. Improved limb salvage and regeneration with angiogenesis induced by PFA scaffold

The therapeutic potential toward angiogenesis based on PFA scaffold containing cells was verified by *in vivo* hindlimb ischemia model. Angiogenic potency of PFA scaffold containing cells by forming tubular morphology of HUVECs *in vitro* was proved in the ischemic hindlimb lesion with attenuated limb salvage ratio and reduced muscle degeneration. The angiogenic effect of PFA scaffold containing cells was proved by analyzing inflammation, muscle degeneration, and limb loss ratio. Morphological and histological analysis revealed superior outcomes in mice treated with the PFA scaffold combined with HUVECs and ADSCs, 28 days post-treatment, compared to other groups (Fig. 6). Mice treated with PFA scaffold containing cells showed decreased ratio of toe necrosis and foot loss with higher limb salvage compared to other groups (Fig. 6A). Half of the mice showed limb salvage in PFA scaffold containing cells implanted group. Limb tissues retrieved from ischemic lesion analyzed histologically to observe inflammation and muscle degeneration (Fig. 6B and C) showed that PFA scaffold containing cells had minimal fibrosis with sparse collagen fibers, reflecting a reduced

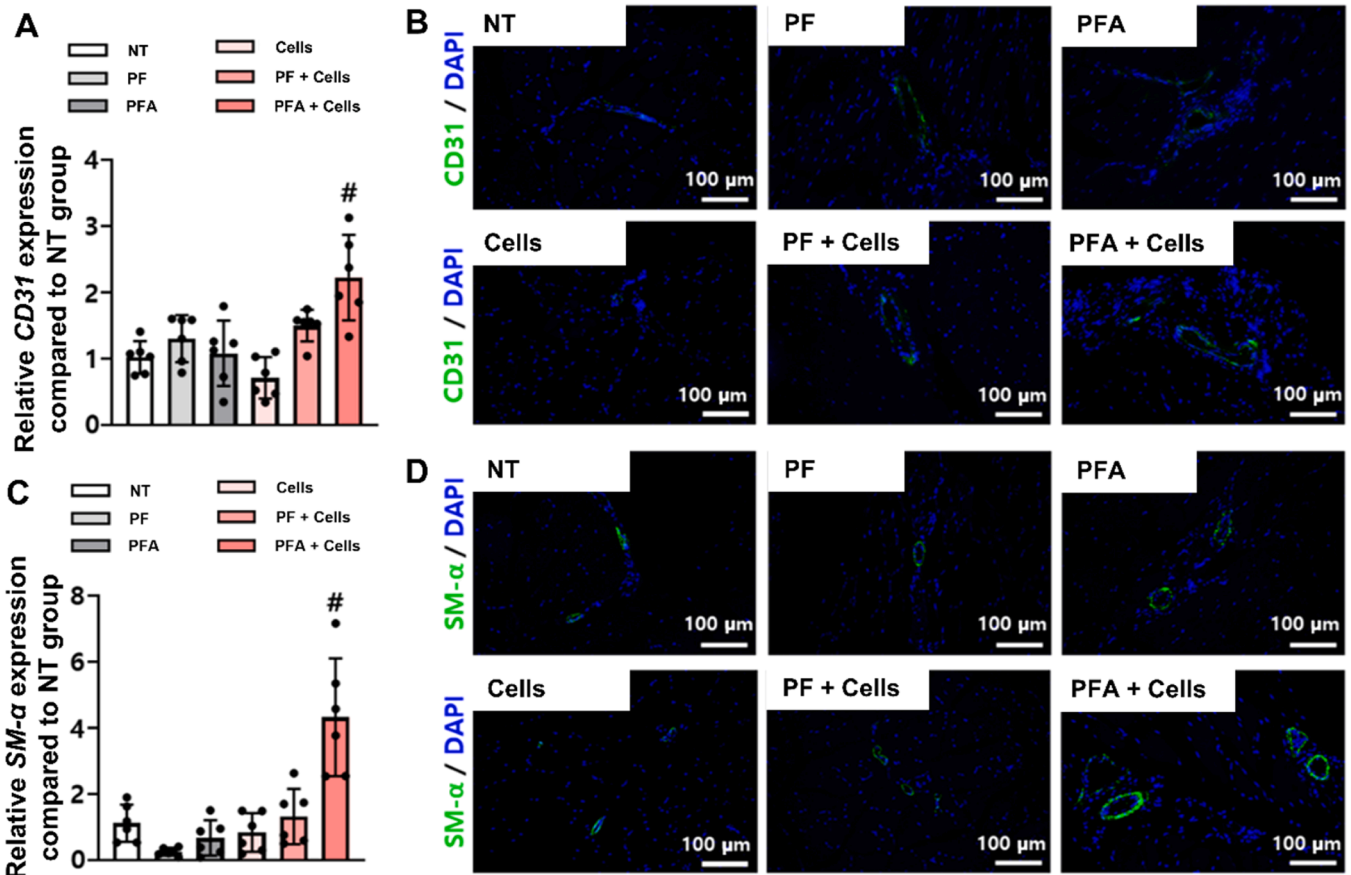


Fig. 7. Enhanced angiogenesis in ischemic hindlimb lesion at 28 days after treating PFA scaffold. (A) Relative gene expression of *CD31* in ischemic lesions ($\#p < 0.05$ compared to other groups, $n = 6$). (B) Representative images of immunohistochemistry stained with *CD31* (green) in ischemic lesions. Scale bars = 100 μm . (C) Relative gene expression of *SM α -actin* in ischemic lesions ($\#p < 0.05$ compared to other groups, $n = 6$). (D) Representative images of immunohistochemistry stained with *SM α -actin* (green) in ischemic lesions. Scale bars = 100 μm . (NT: no treatment, PF: PF scaffold only, PFA: PFA scaffold only, Cells: HUVECs + ADSCs, PF + Cells: PF scaffold with HUVECs + ADSCs, PFA + Cells: PFA scaffold with HUVECs + ADSCs).

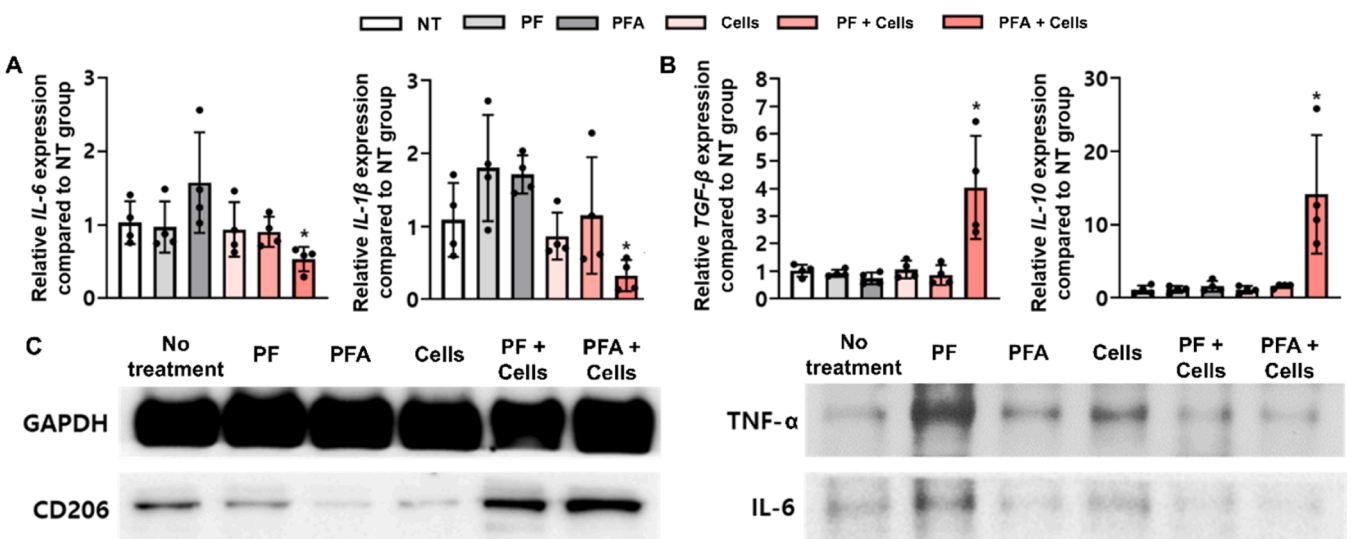


Fig. 8. Immune modulatory effect of PFA scaffold in ischemic hindlimb lesion at 3 days after the surgery. (A) Relative gene expression of M1 macrophage marker (*IL-6* and *IL-1 β*) in ischemic lesions ($n = 4$, $*p < 0.05$ compared to no treatment). (B) Relative gene expression of M2 macrophage marker (*TGF- β* and *IL-10*) in ischemic lesions ($n = 4$, $*p < 0.05$ compared to no treatment). (C) Representative images of western blot analysis for M1 macrophage marker (*CD206*) expression. (NT: no treatment, PF: PF scaffold only, PFA: PFA scaffold only, Cells: HUVECs + ADSCs, PF + Cells: PF scaffold with HUVECs + ADSCs, PFA + Cells: PFA scaffold with HUVECs + ADSCs).

fibrotic response with better preservation of muscle architecture compared to the other groups.

PFA scaffold containing cells led promoted micro blood vessel formation in the ischemic hindlimb lesion. To confirm the angiogenic effect of PFA scaffold containing cells on reduced tissue damage, limb tissues retrieved from the ischemic lesion were analyzed. Representative angiogenesis, CD31 and SM α -actin, were analyzed by gene and protein expression. Relative gene expression of *CD31* and *SM α -actin* showed significant upregulation in mice treated with PFA scaffold containing cells compared to all other groups (qRT-PCR, Fig. 7A and C). Additionally, immunohistochemical staining for angiogenesis in the ischemic lesion based on CD31 and SM α -actin expression was performed (Fig. 7B and D). Enhanced green signals indicating the expression of CD31 and SM α -actin were observed in mice treated with PFA scaffold containing cells compared to other groups. Taken together, the mice treated with PFA scaffold containing cells showed attenuated muscle degeneration and fibrosis due to promoted angiogenesis.

3.6. In vivo immune modulatory effect of PFA scaffold

PFA scaffold containing cells modulated the immune system in mice with lower expression of M1 macrophage-related marker expression and higher expression of M2 macrophage-related marker expression at gene level and protein level. Immune modulatory effect of PFA scaffold containing cells was ascertained by quantitative and qualitative analysis based on M1- and M2-macrophage marker expressions. Relative gene expression of M1- and M2-macrophage markers in the ischemic hindlimb lesion were evaluated by qRT-PCR (Fig. 8A and B). Mice treated with PFA scaffold containing cells showed significantly downregulated *IL-6* and *IL-1 β* expression compared to no treatment, whereas M2 macrophage markers including *TGF- β* and *IL-10* were overexpressed in PFA scaffold containing cells treated mice. Similar patterns were observed in protein expression as detected in gene expression (Fig. 8C). M1 macrophage related protein (TNF- α and IL-6) expression was reduced in mice treated with PFA scaffold containing cells, whereas M2 macrophage related protein (CD206) expression was promoted. The modulated immune responses concluded from the gene and protein levels can be attributed to the anti-inflammatory and antioxidant properties of alginate scaffold. Due to the encapsulation effect of alginate, the release of immunogenic substances, such as fibrinogen, a component of fibrin gel fragments, was suppressed [51]. This suppression likely contributed to the observed anti-inflammatory response, which can be attributed to the intrinsic anti-inflammatory properties of the stem cells [52]. This might help maintaining a balance between pro-inflammatory and anti-inflammatory signals, promoting tissue repair and regeneration. We also observed that ADSCs exhibit a significant anti-inflammatory response by reducing pro-inflammatory cytokine, IL-6 and IL-1 β and promoting the differentiation of macrophages into the M2 phenotype, suggesting the cocktail used effectively harnesses ADSCs property to mitigate inflammation [53]. The significant modulation of cytokine levels by the PFA scaffold containing cells highlights its potential for effectively managing immune responses, which is crucial for preventing chronic inflammation and enhancing tissue healing in regenerative medicine.

4. Conclusion

This study introduces a multilayered PCL-fibrin-alginate hydrogel scaffold with significant potential for treating hindlimb ischemia. By integrating mechanical strength, cellular support, and immune modulation, this scaffold establishes a stable environment that not only promotes vascular network formation but also mitigates inflammation—addressing critical challenges in ischemic tissue repair. The co-culture of ADSCs and HUVECs within the scaffold enhances angiogenic signaling and fosters a regenerative environment supportive of sustained healing. The encouraging in vitro and in vivo results,

including improved tissue integrity, reduced inflammatory response, and increased limb salvage rates, underscore the scaffold's suitability for future ischemia therapies and its promise for broader applications in regenerative medicine.

CRedit authorship contribution statement

Lee Kangwon: Supervision, Resources, Project administration, Funding acquisition. **Kim Yeong Hwan:** Writing – original draft, Methodology, Investigation, Data curation, Conceptualization. **Kim Dongwoo:** Methodology, Investigation, Data curation. **Lee Dong-Hyun:** Writing – review & editing, Validation, Investigation, Data curation. **Bhang Suk Ho:** Supervision, Resources, Project administration, Funding acquisition. **Lee Gyubok:** Writing – original draft, Visualization, Methodology, Investigation, Formal analysis, Data curation, Conceptualization.

Declaration of Competing Interest

The authors declare that they have no known competing financial interests or personal relationships that could have appeared to influence the work reported in this paper.

Acknowledgements

This research was supported by a grant of Ministry of Trade, Industry, and Energy, Republic of Korea (No. 20018522), and a grant of Korea Health Technology R&D Project through the Korea Health Industry Development Institute (KHIDI), funded by the Ministry of Health and Welfare, Republic of Korea (No. HI22C1394). This work has been financially supported by Korean Fund for Regenerative Medicine (KFRM) grant funded by the Korea government (the Ministry of Science and ICT, the Ministry of Health & Welfare; project Number: 21A0102L1-12) and the KIST Institutional Program (Project No. 2E32351, 2E32350 “Development of cellular bloc platform technology”, Korea).

Appendix A. Supporting information

Supplementary data associated with this article can be found in the online version at doi:10.1016/j.colsurfb.2025.114553.

Data availability

Data will be made available on request.

References

- [1] A. Trounson, C. McDonald, Stem cell therapies in clinical trials: progress and challenges, *Cell Stem Cell* 17 (1) (2015) 11–22.
- [2] W. Zakrzewski, M. Dobrzynski, M. Szymonowicz, Z. Rybak, Stem cells: past, present, and future, *Stem Cell Res. Ther.* 10 (1) (2019) 68.
- [3] J.M. Gimble, A.J. Katz, B.A. Bunnell, Adipose-derived stem cells for regenerative medicine, *Circ. Res.* 100 (9) (2007) 1249–1260.
- [4] B.A. Bunnell, M. Flaata, C. Gagliardi, B. Patel, C. Ripoll, Adipose-derived stem cells: isolation, expansion and differentiation, *Methods* 45 (2) (2008) 115–120.
- [5] J.K. Fraser, R. Schreiber, B. Strem, M. Zhu, Z. Alfonso, I. Wulur, M.H. Hedrick, Plasticity of human adipose stem cells toward endothelial cells and cardiomyocytes, *Nat. Clin. Pract. Cardiovasc. Med.* 3 (1) (2006) S33–S37.
- [6] G.E. Kilroy, S.J. Foster, X. Wu, J. Ruiz, S. Sherwood, A. Heifetz, J.W. Ludlow, D. M. Stricker, S. Potiny, P. Green, Y.-D.C. Halvorsen, B. Cheatham, R.W. Storms, J. M. Gimble, Cytokine profile of human adipose-derived stem cells: expression of angiogenic, hematopoietic, and pro-inflammatory factors, *J. Cell. Physiol.* 212 (3) (2007) 702–709.
- [7] E.Y. Lee, Y. Xia, W.S. Kim, M.H. Kim, T.H. Kim, K.J. Kim, B.S. Park, J.H. Sung, Hypoxia-enhanced wound-healing function of adipose-derived stem cells: increase in stem cell proliferation and up-regulation of VEGF and bFGF, *Wound Repair Regen.* 17 (4) (2009) 540–547.
- [8] P.A. Zuk, M. Zhu, H. Mizuno, J. Huang, J.W. Futrell, A.J. Katz, P. Benham, H. P. Lorenz, M.H. Hedrick, Multilineage cells from human adipose tissue: implications for cell-based therapies, *Tissue Eng.* 7 (2) (2001) 211–228.

- [9] J.M. Gimble, F. Guilak, B.A. Bunnell, Clinical and preclinical translation of cell-based therapies using adipose tissue-derived cells, *Stem Cell Res. Ther.* 1 (2) (2010) 19.
- [10] N.F. Huang, S. Li, Mesenchymal stem cells for vascular regeneration, *Regen. Med.* 3 (6) (2008) 877–892.
- [11] J.B. Lee, D.H. Kim, J.K. Yoon, et al., Microchannel network hydrogel induced ischemic blood perfusion connection, *Nat. Commun.* 11 (2020) 615.
- [12] T. Hao, M. Qian, Y. Zhang, Q. Liu, A.C. Midgley, Y. Liu, Y. Che, J. Hou, Q. Zhao, An injectable dual-function hydrogel protects against myocardial ischemia/reperfusion injury by modulating ROS/NO disequilibrium, *Adv. Sci.* 9 (2022) e2105408.
- [13] Y.-C. Chen, R.-Z. Lin, H. Qi, Y. Yang, H. Bae, J.M. Melero-Martin, A. Khademhosseini, Functional human vascular network generated in photocrosslinkable gelatin methacrylate hydrogels, *Adv. Funct. Mater.* 22 (2012) 2027–2039.
- [14] X. Zhang, W. Liu, Engineering injectable anti-inflammatory hydrogels to treat acute myocardial infarction, *Adv. NanoBiomed Res.* 2 (2022) 2200008.
- [15] S. Yamanaka, Induced pluripotent stem cells: past, present, and future, *Cell Stem Cell* 10 (6) (2012) 678–684.
- [16] N. Amariglio, A. Hirshberg, B.W. Scheithauer, Y. Cohen, R. Loewenthal, L. Trakhtenbrot, N. Paz, M. Koren-Michowitz, D. Waldman, L. Leider-Trejo, A. Toren, S. Constantini, G. Rechavi, Donor-derived brain tumor following neural stem cell transplantation in an ataxia telangiectasia patient, *PLoS Med.* 6 (2) (2009) e1000029.
- [17] E.S. Place, J.H. George, C.K. Williams, M.M. Stevens, Synthetic polymer scaffolds for tissue engineering, *Chem. Soc. Rev.* 38 (4) (2009) 1139–1151.
- [18] A.S. Hoffman, Hydrogels for biomedical applications (Suppl), *Adv. Drug Deliv. Rev.* 64 (2012) 18–23.
- [19] G. Long, Q. Wang, S. Li, J. Tao, B. Li, X. Zhang, X. Zhao, Engineering of injectable hydrogels associate with Adipose-Derived stem cells delivery for anti-cardiac hypertrophy agents, *Drug Deliv.* 28 (1) (2021) 1334–1341.
- [20] N. Kohli, V. Sharma, A. Orera, P. Sawadkar, N. Owji, O.G. Frost, J.S. Birch, E. T. Pijuan-Galitó, A.J. El Haj, K.M. Shakesheff, L.J. White, Pro-angiogenic and osteogenic composite scaffolds of fibrin, alginate and gelatin for bone tissue engineering, *J. Tissue Eng.* 12 (2021), 20417314211005610.
- [21] M.A. Woodruff, D.W. Hutmacher, The return of a forgotten polymer—Polycaprolactone in the 21st century, *Prog. Polym. Sci.* 35 (10) (2010) 1217–1256.
- [22] N. Recek, M. Resnik, H. Motaln, T. Lah-Turnšek, R. Augustine, N. Kalarikkal, S. Thomas, M. Mozetič, Cell adhesion on polycaprolactone modified by plasma treatment, *Int. J. Polym. Sci.* 2016 (2016) 7354396.
- [23] K. Gholivand, M. Mohammadpour, S.A. Alavinasab Ardebili, R. Eshaghi Malekshah, H. Samadian, Fabrication and examination of polyorganophosphazene/polycaprolactone-based scaffold with degradation, in vitro and in vivo behaviors suitable for tissue engineering applications, *Sci. Rep.* 12 (2022) 18407.
- [24] P.A. Janmey, J.P. Winer, J.W. Weisel, Fibrin gels and their clinical and bioengineering applications, *J. R. Soc. Interface* 6 (30) (2009) 1–10.
- [25] X. Feng, M.G. Tonnesen, S.A. Mousa, R.A. Clark, Fibrin and collagen differentially but synergistically regulate sprout angiogenesis of human dermal microvascular endothelial cells in 3-dimensional matrix, *Int. J. Cell Biol.* 2013 (2013) 231279.
- [26] N. Laurens, M.A. Engelse, C. Jungerius, C.W. Löwik, V.W. van Hinsbergh, P. Koolwijk, Single and combined effects of α 5 β 1- and α 5 β 1-integrins on capillary tube formation in a human fibrous matrix, *Angiogenesis* 12 (3) (2009) 275–285.
- [27] L. Yang, X. Li, D. Wang, S. Mu, W. Lv, Y. Hao, X. Lu, G. Zhang, W. Nan, H. Chen, L. Xie, Y. Zhang, Y. Dong, Q. Zhang, L. Zhao, Improved mechanical properties by modifying fibrin scaffold with PCL and its biocompatibility evaluation, *J. Biomater. Sci. Polym. Ed.* 31 (2020) 658–678.
- [28] A. King, Microencapsulation of islets of Langerhans: impact of cellular overgrowth, *Ups. J. Med. Sci.* 106 (3) (2001) 161–174.
- [29] X. Chen, T. Wu, Y. Bu, H. Yan, Q. Lin, Fabrication and biomedical application of alginate composite hydrogels in bone tissue engineering: a review, *Int. J. Mol. Sci.* 25 (2024) 7810.
- [30] S. Sakai, K. Hirose, K. Moriyama, K. Kawakami, Control of cellular adhesiveness in an alginate-based hydrogel by varying peroxidase and H₂O₂ concentrations during gelation, *Acta Biomater.* 6 (2010) 1446–1452.
- [31] C.E. Vorwald, T. Gonzalez-Fernandez, T.G. Fang, P.C. Caracciolo, J.K. Leach, Tunable fibrin-alginate interpenetrating network hydrogels to support cell spreading and network formation, *Acta Biomater.* 110 (2020) 153–165.
- [32] H.R. Moyer, R.C. Kinney, K.A. Singh, J.K. Williams, Z. Schwartz, B.D. Boyan, Alginate microencapsulation technology for the percutaneous delivery of adipose-derived stem cells, *Ann. Plast. Surg.* 65 (5) (2010) 497–503.
- [33] A. Pangjantuk, P. Kaokaen, P. Kunhorm, N. Chaicharoenudomrung, P. Noisa, 3D culture of alginate-hyaluronic acid hydrogel supports the stemness of human mesenchymal stem cells, *Sci. Rep.* 14 (2024) 4436.
- [34] D.O. Traktuev, S. Merfeld-Clauss, J. Li, M. Kolonin, W. Arap, R. Pasqualini, B. H. Johnstone, K.L. March, A population of multipotent CD34-positive adipose stromal cells share pericyte and mesenchymal surface markers, reside in a periendothelial location, and stabilize endothelial networks, *Circ. Res.* 102 (1) (2008) 77–85.
- [35] X. Bai, Y. Yan, Y.H. Song, M. Seidensticker, B. Rabinovich, R. Metzle, J. A. Bankson, D. Vykoukal, E. Alt, Both cultured and freshly isolated adipose tissue-derived stem cells enhance cardiac function after acute myocardial infarction, *Eur. Heart J.* 31 (4) (2010) 489–501.
- [36] M. Gneccchi, Z. Zhang, A. Ni, V.J. Dzau, Paracrine mechanisms in adult stem cell signaling and therapy, *Circ. Res.* 103 (11) (2008) 1204–1219.
- [37] P. Carmeliet, R.K. Jain, Molecular mechanisms and clinical applications of angiogenesis, *Nature* 473 (7347) (2011) 298–307.
- [38] M. Jeyaraman, S. Nagarajan, N. Maffulli, R.P. P. N. Jeyaraman, N. A. M. Khanna, S. Yadav, A. Gupta, Stem cell therapy in critical limb ischemia, *Cureus* 15 (7) (2023) e41772.
- [39] L. Norgren, W.R. Hiatt, J.A. Dormandy, M.R. Nehler, K.A. Harris, F.G.R. Fowkes, Inter-society consensus for the management of peripheral arterial disease (TASC II), *J. Vasc. Surg.* 45 (S) (2007) S5–S67.
- [40] M.K. Mamidi, R. Pal, S. Dey, B.J.J. Bin Abdullah, Z. Zakaria, M.S. Rao, A.K. Das, Cell therapy in critical limb ischemia: current developments and future progress, *Cytotherapy* 14 (8) (2012) 902–916.
- [41] X. Zhao, Q. Li, Z. Guo, Constructing a cell microenvironment with biomaterial scaffolds for stem cell therapy, *Stem Cell Res. Ther.* 12 (1) (2021) 583.
- [42] Y. Wang, R.K. Kankala, C. Ou, A. Chen, Z. Yang, Advances in hydrogel-based vascularized tissues for tissue repair and drug screening, *Bioact. Mater.* 9 (2021) 198–220.
- [43] Z. Ghanavati, M. Orazizadeh, V. Bayati, M.R. Abbaspour, L. Khorsandi, E. Mansouri, N. Neisi, Characterization of a three-dimensional organotypic coculture skin model for epidermal differentiation of rat adipose-derived stem cells, *Cell J.* 18 (3) (2016) 289–301.
- [44] Y. Yuan, Z. Zhang, F. Mo, C. Yang, Y. Jiao, E. Wang, Y. Zhang, P. Lin, C. Hu, W. Fu, J. Chang, L. Wang, A biomaterial-based therapy for lower limb ischemia using Sr/Si bioactive hydrogel that inhibits skeletal muscle necrosis and enhances angiogenesis, *Bioact. Mater.* 26 (2023) 264–278.
- [45] S.K. Gopal, D.W. Greening, H.-J. Zhu, R.J. Simpson, R.A. Mathias, Transformed MDCK cells secrete elevated MMP1 that generates LAMA5 fragments promoting endothelial cell angiogenesis, *Sci. Rep.* 6 (2016) 28321.
- [46] H. Chen, P. Jia, H. Kang, H. Zhang, Y. Liu, P. Yang, Y. Yan, G. Zuo, L. Guo, M. Jiang, J. Qi, Y. Liu, W. Cui, H.A. Santos, L. Deng, Upregulating Hif-1 α by hydrogel nanofibrous scaffolds for rapidly recruiting angiogenesis relative cells in diabetic wound, *Adv. Healthc. Mater.* 5 (8) (2016) 907–918.
- [47] H. Mutschall, S. Winkler, V. Weisbach, A. Arkudas, R.E. Horch, D. Steiner, Bone tissue engineering using adipose-derived stem cells and endothelial cells: effects of the cell ratio, *J. Cell. Mol. Med.* 24 (12) (2020) 7034–7043.
- [48] Z. Shen, W. Wang, J. Chen, B. Chen, Y. Tang, J. Hou, J. Li, S. Liu, Y. Mei, L. Zhang, S. Lu, Small extracellular vesicles of hypoxic endothelial cells regulate the therapeutic potential of adipose-derived mesenchymal stem cells via miR-486-5p/PTEN in a limb ischemia model, *J. Nanobiotechnol.* 20 (1) (2022) 422.
- [49] V. Vaithilingam, C. Fung, S. Ratnapala, J. Foster, V. Vaghjiani, U. Manuelpillai, B. E. Tuch, Characterisation of the xenogeneic immune response to microencapsulated fetal pig islet-like cell clusters transplanted into immunocompetent C57BL/6 mice, *PLoS One* 8 (3) (2013) e59120.
- [50] M. Yanez, J. Blanchette, E.B. Jabbarzadeh, Modulation of inflammatory response to implanted biomaterials using natural compounds, *Curr. Pharm. Des.* 23 (41) (2017) 6347–6357.
- [51] T. Jensen, P. Kierulf, P.M. Sandset, O. Klingenberg, G.B. Jøø, H.C. Godal, O. H. Skjønberg, Fibrinogen and fibrin induce synthesis of proinflammatory cytokines from isolated peripheral blood mononuclear cells, *Thromb. Haemost.* 97 (5) (2007) 822–829.
- [52] Z. Liu, N. Xu, M. Wang, R. Tang, X. Liu, Physical confinement in alginate cryogels determines macrophage polarization to a M2 phenotype by regulating a STAT-related mRNA transcription pathway, *Biomater. Sci.* 10 (9) (2022) 2315–2327.
- [53] T. Kotani, R. Masutani, T. Suzuka, K. Oda, S. Makino, M. Ii, Anti-inflammatory and anti-fibrotic effects of intravenous adipose-derived stem cell transplantation in a mouse model of bleomycin-induced interstitial pneumonia, *Sci. Rep.* 7 (2017) 14608.